Photodissociation of Formyl Fluoride in Rare Gas Matrixes

Jussi M. E. Ahokas, Kari J. Vaskonen, and Henrik M. Kunttu*

Nanoscience Center, Department of Chemistry, P.O. Box 35, 40014 University of Jyväskylä, Finland

Received: January 13, 2006; In Final Form: March 27, 2006

Photodissociation of formyl fluoride (HCOF) is studied in Ar, Kr, and Xe matrixes at 248 and 193 nm excitation by following spectral changes in the infrared absorption spectra. In all matrixes, the main photodissociation products are CO/HF species, including CO−HF and OC−HF complexes and thermally unstable CO/HF species (a distorted CO/HF complex or a reaction intermediate), which indicate negligible cage exit of atoms produced via the C−F and C−H bond cleavage channels. However, the observation of traces of H, F, CO, CO_2, F_2CO, FCO, and HRg_2^+ (Rg = Kr or Xe) in Kr and Xe matrixes would imply some importance of other reaction channels too. The analysis of the decay curves of the precursor shows that dissociation efficiency of HCOF increases as Ar < Kr < Xe, the difference being the factor of 10 between Ar and Xe. Moreover, HCOF dissociates 20−50 times faster at 193 nm compared to 248 nm. Interestingly, whereas the CO/HF species are stable with respect to photolysis in Ar, they photobleach in Kr and Xe matrixes at 248 and 193 nm, even though the first excited states of CO and HF are not energetically accessible with 193 and 248 nm photons. In krypton matrix, the photodissociation of CO/HF species at 248 nm is observed to be a single photon process. Quantum chemical calculations of electronic excitation energies of CO−HF and OC−HF complexes show that the electronic states of HF and CO mostly retain their diatomic nature in the pair. This clearly demonstrates that photodissociation of CO/HF complexes is promoted by the surrounding rare gas lattice.

Introduction

Photodissociation dynamics of formyl fluoride (HCOF) embedded in solid rare gas matrixes can provide insights into condensed phase effects on photodissociation of polyatomic molecules. Because of its electronic and structural properties, HCOF serves as a prototype for studying multichannel unimolecular dissociation. Moreover, the results may be directly compared with the results obtained from studies on photodissociation of formaldehyde (H_2CO), which has been widely studied in the gas phase[1] and condensed phases.[2,3]

Extensive experimental and theoretical interest has been focused on photodissociation of HCOF in the gas phase, not only from purely academic interest but due to its role in atmospheric chemistry as well.[4] Ultraviolet (UV) light excitation of HCOF enables several photodissociation channels in the gas phase:

$$\mathrm{HCOF} \rightarrow \mathrm{HF}(\mathrm{X}\,^1\Sigma^+) + \mathrm{CO}(\mathrm{X}\,^1\Sigma^+) \quad (1)$$

$$\rightarrow \mathrm{H}(^2\mathrm{S}) + \mathrm{FCO}(\mathrm{X}\,^2\mathrm{A}') \quad (2)$$

$$\rightarrow \mathrm{F}(^2\mathrm{P}) + \mathrm{HCO}(\mathrm{X}\,^2\mathrm{A}') \quad (3)$$

$$\rightarrow \mathrm{H}(^2\mathrm{S}) + \mathrm{F}(^2\mathrm{P}) + \mathrm{CO}(\mathrm{X}\,^1\Sigma^+) \quad (4)$$

The existence of channel 1 upon UV photolysis (λ > 165 nm) has been observed by Klimek and Berry.[5] Dissociation to molecular products HF and CO was expected to proceed via highly excited vibrational levels of the ground electronic surface (S_0), and an energy barrier of 205 kJ/mol was estimated.[6] Weiner and Rosenfeld studied photodissociation of HCOF at 248 and 193 nm using time-resolved CO laser spectroscopy.[7] They concluded the existence of the two bond fission channels 2 and 3 at both wavelengths, and showed some evidence of dissociation channel 4 upon 193 nm photoexcitation. A dissociation energy of 418 kJ/mol for the C−H bond fission and an upper limit of 482 kJ/mol for the C−F bond fission were obtained from photofragment translational spectroscopy experiments in the excitation wavelength range 218.2−248.2 nm (548−482 kJ/mol).[8−10]

The radiationless decay of the initially excited first electronic singlet state (S_1) of HCOF can proceed via different routes. Internal conversion (IC) to the singlet ground state (S_0) is involved in channel 1,[7] whereas photodissociation via channels 2 and 3 has been ascribed to intersystem crossing (ISC) to the T_1 surface, and subsequent passage over the energy barrier (or through it by tunneling) to the T_1 product asymtote.[8] The ratio of the rate coefficients for channels 2 and 3 on the T_1 surface is 42.4:1.0 as obtained from RRKM calculation.[11] Furthermore, theoretical investigations indicate that the C−F bond fission is more favorable on the S_1 surface at excitation wavelengths shorter than 233 nm.[11] This is in accordance with the experimental H atom time-of-flight spectra, in which the faster H atom signal was assigned to secondary dissociation of HCO at excitation wavelengths shorter than 233 nm.[9]

Recently, Lee et al. have studied photodissociation dynamics of HCOF in the gas phase at 193 nm excitation.[12] They found that the C−F and C−H bond fission channels have branching ratios of ∼0.66 and ∼0.28, respectively. Comparison of the experimentally observed branching ratios with theoretical ones clearly demonstrates that the C−F bond fission most likely proceeds on the initially excited S_1 state, whereas the C−H bond fission proceeds via the T_1 surface.[11] On the other hand, the molecular channel, which proceeds via the S_0 surface, has a branching ratio of ∼0.06.

To the best of our knowledge, there is only one previous experimental study on photochemistry of HCOF in rare gas

* Corresponding author. e-mail: hekunttu@jyu.fi.

10.1021/jp060249o CCC: $33.50
Published on Web 04/25/2006

matrixes. Shatte et al. studied photodissociation of HCOF in argon matrix by medium-pressure mercury arc photolysis and focused on the formation of molecular complex between CO and HF.[13] The linear molecular complexes OC−HF and CO−HF as well as one thermally unstable CO/HF species were observed as the primary products upon photolysis, and only a very small fraction of HF and CO was observed to escape from the matrix cage. Hereafter, the term CO/HF complex refers to the molecular complexes of OC−HF and CO−HF. The structure of the thermally unstable CO/HF species was suggested to be linear CO/HF complex with argon vacancies nearby and/or CO/HF π-complex.[13] The term CO/HF species refers to the thermally unstable CO/HF species and the CO/HF complexes.

In this paper, we present the results of studies on UV photodissociation of HCOF at 248 and 193 nm in argon, krypton, and xenon matrixes. The results are compared with the gas-phase studies and the effects of solid environment on photodissociation are discussed. The photochemistry of CO/HF molecular complexes is reported as well. Ab initio CIS, EOM-CCSD, and TD-B3LYP DFT calculations are carried out to estimate vertical excitation energies of the photoproducts.

Experimental Details

Formyl fluoride was prepared from formic acid (Riedel-de Haën), benzoyl chloride (Merck), and potassium hydrogen fluoride (Aldrich), according to the method by Olah and Kuhn,[14] and purified by low temperature distillation. The pure formyl fluoride was stored in a Pyrex bulb and kept under liquid nitrogen. Formyl fluoride was mixed in a vacuum line with argon (Aga, 99.9999%), krypton (Aga, 99.997%), or xenon (Aga, 99.997%) prior to matrix isolation experiments. The gas mixtures were deposited onto a low temperature CsI substrate attached to the coldfinger of a closed-cycle helium cryostat (APD Cryogenics, DE-202A). The deposition rate was typically ca. 0.06 mmol/min and the total amount of the deposit was 4−8 mmol. Temperature of the substrate was held at 15−35 K during deposition, and all matrixes were subject to annealing at 35−40 K (Ar), 40 K (Kr), and 50 K (Xe) prior to spectral measurements and photolysis at 10 K. The cryostat was equipped with CsI windows for infrared measurements and a MgF_2 window for UV photolysis.

Infrared spectra were collected with a Nicolet Magna IR 760 spectrometer equipped with a HgCdTe detector and a KBr beam splitter. The spectral resolution was 0.125−0.5 cm^{-1}. ArF and KrF excimer lasers (Lambda Physik, Optex) were used to photolyze the samples.

An Oriel MS125 spectrograph equipped with an Andor ICCD detector was used to record the UV absorption spectra. A deuterium lamp (Opthos) was used as a light source.

Computational Details

Ab initio calculations were performed using Gaussian 03 (Revision C.02)[15] and Gamess (US)[16] packages. All geometry optimizations and calculation of harmonic frequencies were carried out at the SCF, B3LYP, and CCSD levels using Gaussian 03.[17,18] Vertical excitation energies were performed at the CIS and TD-B3LYP levels using Gaussian 03 and at EOM-CCSD level using Gamess (US).[19−21] 6-311++G** basis set was used for all atoms.[22]

Experimental Results

IR Observations. The relatively high ability of HCOF to form aggregates in low temperature matrixes caused problems in sample preparation. Deposition of dilute samples at relatively low temperature produced monomeric matrixes but their optical quality was often unsatisfactory for the experiments. For this reason, matrixes were grown in conditions where dimers and higher aggregates were present in some extent, but the matrixes were of acceptable optical quality.

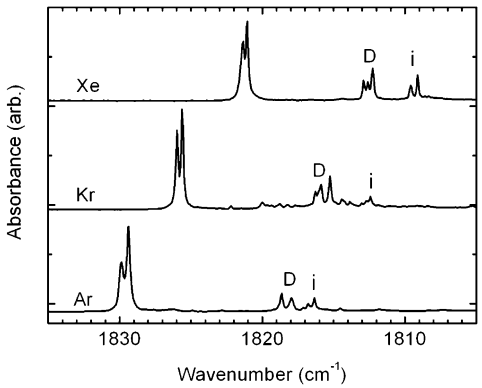

Figure 1. CO stretching region of HCOF in argon, krypton, and xenon matrixes. Dimer bands are marked with D, and i indicates HCOF bands, which are most probably induced by an impurity or higher aggregates.

To obtain reasonable monomeric trapping of HCOF in argon matrix, a HCOF/Ar = 1/2000 gas sample was deposited at 15 K. The IR absorption spectrum of HCOF in argon matrix was assigned according to Shatte et al.[13] The absorptions bands of ν_1 (CH stretching), ν_2 (CO stretching), ν_4 (CF stretching), and ν_5 (FCO bending) vibrational modes were all split into two components. The absorption band of the CF stretching mode was accompanied by shoulder bands at 1056.4 and 1055.4 cm^{-1}. Two peaks corresponding to the weak ν_3 (HCF bending) mode were observed at 1342.86 and 1344.03 cm^{-1}. The very weak absorption of ν_6 (out-of-plane bending) could not be reliably identified. Additionally to the HCOF monomer, peaks belonging to the CO stretching and HCF bending modes of $(HCOF)_2$,[13] as well as some traces of carbon monoxide and water, were observed in the spectrum. The source for CO is obviously decomposition of HCOF on the walls of the stainless steel capillary of the deposition system. Other absorptions appeared at 1033.50, 1816.35, and 1816.78 cm^{-1} and a number of weak absorptions within ranges 1810−1828 and 2130−2160 cm^{-1}. These absorptions are discussed in more detail in ref 23.

Reasonable monomeric trapping of HCOF in krypton and xenon matrixes was obtained when the gas mixture with dilution ratio of 1/2000 was deposited at 20 and 35 K, respectively. The CO stretching bands of HCOF in argon, krypton, and xenon matrixes are shown in Figure 1. The spectral features are similar in all matrixes and show typical matrix shifts. The observed IR absorptions of HCOF are collected in Table 1.

Photodissociation rates of HCOF were studied at 248 and 193 nm by utilizing KrF and ArF excimer laser photolysis. The result of the photolysis in argon matrix at 248 nm is shown in Figure 2 as a difference IR spectrum. All initial IR absorptions, except those of water and CO, were completely bleached upon irradiation, and absorptions of new photoproducts were observed in ranges between 3700 and 3910 cm^{-1}, between 2100 and 2200 cm^{-1}, and around 420 cm^{-1}. No indication of radical products HCO and FCO could be seen in the spectrum, and the amount of monomeric carbon monoxide increased slightly.

The new absorptions between 3700 and 3910 cm^{-1} due to photoproducts are shown in Figure 3 along with spectra of a subsequently annealed sample. The absorptions of the photodissociation products appeared at 3771.84, 3773.12, 3774.56, 3775.36, 3789.58, 3795.80, 3797.94, 3908.44, and 3911.54

TABLE 1: IR Absorptions of HCOF in Argon, Krypton, and Xenon Matrixes

Ar	Kr	Xe	assignment[a]
2995.95/2996.74	2987.31/2988.65	2974.59/2975.83	ν_1(CH-str)
1829.39/1829.90	1825.62/1825.98	1821.07/1821.34	ν_2(CO-str)
1342.83/1344.07 (?)	1339.69 (w)	1336.33 (w)	ν_3(HCF-bend)
1055.81/1056.51	1051.90/1052.59	1047.14	ν_4(CF-str)
664.36/664.58	663.48/663.80	661.76/662.05	ν_5(FCO-bend)
3637.69/3638.71	3630.12/3630.82	3620.95/3621.43	$2\nu_2$
2097.25	2089.28	2079.65	$2\nu_4$
1712.25			$\nu_4 + \nu_5$
672.79	671.48	668.58	$(HCOF)_2$ ν(FCO-bend)
1817.95/1818.65			$(HCOF)_2$ ν(CO-bend)
2138.55	2135.69	2133.09	CO

[a] See refs 13 and 24.

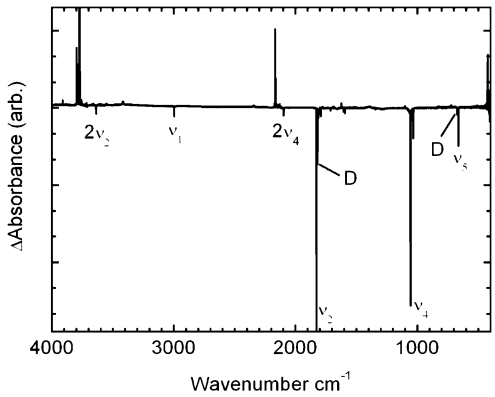

Figure 2. Difference spectrum of HCOF/Ar (1:2000) matrix upon photolysis at 248 nm. Upward signals indicate the formation of photoproducts. D indicates dimer band locations.

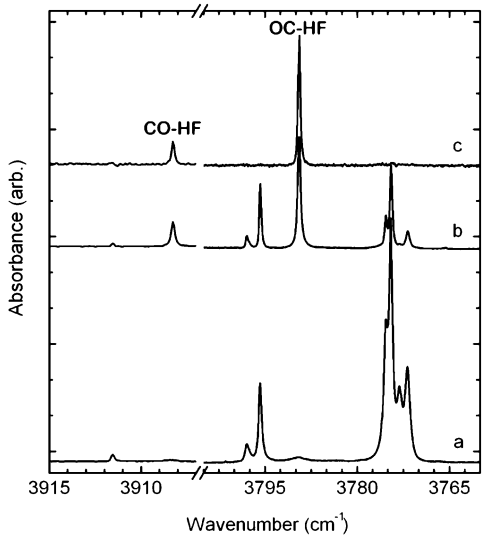

Figure 3. IR spectra of the products formed in the photolysis of HCOF in an argon matrix, after photolysis at 248 nm (a), with subsequent annealing at 35 K (b), and at 40 K (c). All spectra are recorded at 10 K.

cm^{-1}. Two weak absorptions at 3789.58 and 3908.44 cm^{-1} belong to the OC−HF and CO−HF complexes, respectively.[13] The absorption at 3773.12 cm^{-1} was thermally unstable at 10 K, and its intensity decreased by a factor of ca. 2 when the sample was left overnight at 10 K. Simultaneously, the absorptions at 3795.80, 3797.94, 3908.44, and 3911.54 cm^{-1} gained intensity. According to Shatte et al. the absorptions at 3775.0 and 3796.0 cm^{-1} belong to a thermally unstable CO/HF species.[13] It should be noted, however, that their assignment was limited by spectral resolution of 1 cm^{-1}. Gradual annealing of the sample bleached all the absorptions except those of OC−HF and CO−HF at 3789.58 and 3908.44 cm^{-1}, respectively, which gained intensity. Additionally, a new absorption appeared at 3713.19 cm^{-1}. Finally, after annealing at 40 K, all absorptions except those of OC−HF and CO−HF and the band at 37013.19 cm^{-1} were completely bleached.

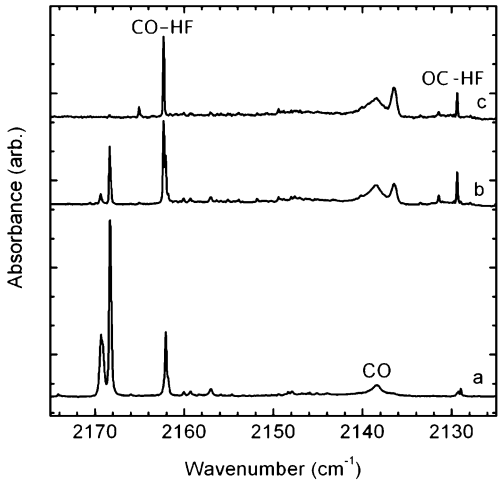

Figure 4. IR spectra of the products formed in the photolysis of HCOF in an argon matrix, after photolysis at 248 nm (a), with subsequent annealing at 35 K (b), and at 40 K (c). All spectra are recorded at 10 K.

The CO stretching region of the CO/HF complexes is shown in Figure 4. After photodissociation, new absorptions appeared at 2128.98, 2129.25 (with red-side shoulder), 2162.07, 2168.32, and 2169.33 cm^{-1} (with red-side shoulder). The red-side shoulder band of the absorption at 2169.33 cm^{-1} was thermally unstable at 10 K, and after overnight storage this absorption lost intensity by a factor of ca. 2. This was accompanied by increase of intensities of the absorptions at 2128.98, 2129.25, and 2162.07 cm^{-1}. Upon gradual annealing of the sample, the absorptions at 2128.98, 2129.25, 2162.07, 2168.32, and 2169.33 cm^{-1} were completely bleached. Simultaneously, the absorptions of CO−HF at 2129.39 cm^{-1} and OC−HF at 2162.31 cm^{-1} appeared,[13] and the absorption of CO slightly increased its intensity, and new absorptions appeared at 2136.49 and 2165.05 cm^{-1}. The absorption at 2136.49 cm^{-1} has been assigned to the CO−N_2 pair.[24]

Photolysis of HCOF in argon matrix at 193 nm yielded the same spectral features as described above for 248 nm photolysis. Additionally, some minor formation of isolated CO and HF was observed. Annealing at 40 K bleached completely the thermally unstable CO/HF species absorptions, and simultaneously, stable CO−HF and OC−HF complexes were formed, and the absorption of CO gained intensity.

Photolysis of HCOF in krypton matrix at 248 nm yielded absorptions at 3793.56, 3790.48, 3750.18, 3748.74, and 3742.68

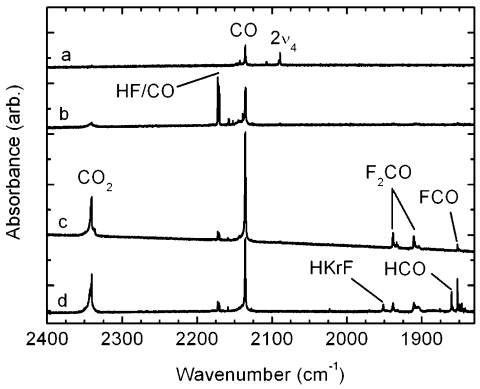

Figure 5. Photolysis of HCOF in a krypton matrix (1/2000) at 248 nm, (a) after deposition at 20 K, (b) after photolysis by 5000 laser pulses, (c) after 45000 laser pulses, and (d) after annealing at 40 K. All spectra are recorded at 10 K.

cm^{-1} in the HF stretching region, and absorptions at 2172.41, 2170.53, 2170.96, and 2157.69 cm^{-1} in the CO stretching region. Annealing at 45 K caused increase of the 3790.48 cm^{-1} absorption, and appearance of new absorptions at 3895, 2158.87, and 2127.45 cm^{-1}. Other absorptions mentioned above bleached upon annealing. As distinct from the argon matrix, photodissociation of HCOF in a krypton matrix yielded a collection of photoproducts. In additional to the CO/HF species absorptions, new absorptions appeared at 3932.31, 1853.04, 1852.36, and 852 cm^{-1} and groups of peaks appeared at 2342, 1938, 1910, 1235, 964, and 766 cm^{-1}. The absorption of CO increased intensity during photolysis.

The absorption at 3932.31 cm^{-1} is assigned to nonrotating monomeric HF, and the absorptions at 1853.04 and 1852.36 cm^{-1} most probably belong to the FCO radical.[25−27] The group of peaks at 1938, 1910, 1235, 964, and 766 cm^{-1} are assigned to the F_2CO molecule.[28] The absorption at 852.45 cm^{-1} has been assigned to the ionic Kr_2H^+ species,[29] and the absorption at 2342 cm^{-1} belongs to CO_2.[30] Prolonged photolysis at 248 nm caused decrease of the CO/HF species absorptions and increase of the absorptions of CO, HF, CO_2, F_2CO, FCO, and Kr_2H^+. Subsequent annealing at 40 K caused decrease of the CO absorption and the absorption of HF was completely bleached. The absorption at 1852.36 cm^{-1} gained intensity, and the absorption of HKrF at 1952 cm^{-1} and another absorption at 1860.36 cm^{-1}, which was assigned to HCO, appeared upon annealing (Figure 5).[31−33] Photolysis of HCOF in a krypton matrix at 193 nm yielded the same photoproduct absorptions as observed at 248 nm photolysis.

Photolysis of HCOF in xenon matrix at 248 and 193 nm yielded CO/HF species absorptions at 3725.73, 2171.43, and 2170.94 cm^{-1}. Similar to the Kr matrix, formation of CO, CO_2, F_2CO, and FCO and the solvation of a proton as Xe_2H^+ species[34] was observed, but no evidence of isolated HF was seen. Also a weak absorption of the HCO radical could be identified. An unassigned absorption at 3886.53 cm^{-1} was red shifted from the monomeric HF absorption,[25] which most probably belongs to the HF complex, but there was no counterpart in the CO stretching region. As in the krypton matrix, the CO/HF species dissociate in the xenon matrix at both photolysis wavelengths.

UV Observations. The UV absorption spectra of the photodissociation products of HCOF were recorded after 193 nm irradiation. A broad neagative signal near 200 nm was characteristic in all matrixes (Figure 6), and resembles the gas-phase UV absorption spectrum of HCOF.[35] In krypton matrix, two intense absorptions at 274 and 234 nm and a weaker absorption

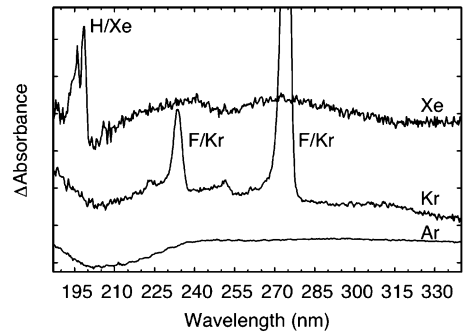

Figure 6. Difference UV absorption spectra recorded after 193 nm photolysis of HCOF in argon, krypton, and xenon matrixes. The broad negative signals around 200 nm are due to bleaching of HCOF.

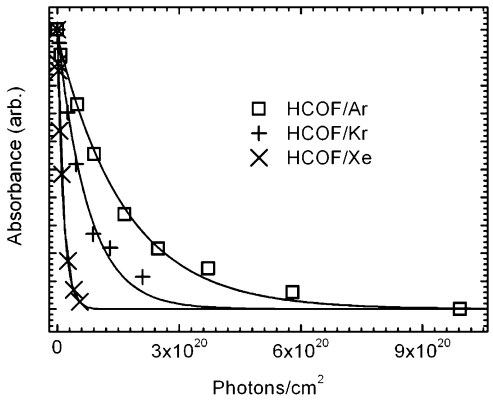

Figure 7. Decay of the IR absorbance of HCOF in Ar, Kr, and Xe matrices in 248 nm photolysis. The experimental data are fitted to first-order kinetics.

at 252 nm of fluorine atom were observed after 193 nm irradiation.[36] The xenon matrix measurements suffered from the poor optical quality of the sample due to low deposition temperature. However, the absorption of hydrogen atom in xenon was observed to overlap with the broad negative absorption.

Kinetic Analysis. The progress of photodissociation of HCOF was followed by monitoring the integrated absorbance of the CH-stretching mode as a function of laser pulses deposited in the sample. For all cases, the rate of disappearance of the precursor obeyed simple first-order kinetics:

$$A = A_0 e^{-kn} \tag{5}$$

where A is the integrated absorbance, $A_0 = A(n = 0)$, n is the number of photons/cm^2 accumulated in the sample, and $k = \sum_i k_i$ represents the effective photodissociation cross section (in cm^2) due to all possible dissociation channels i. In effect, k represents the product of absorption cross-section and dissociation quantum yield. Figure 7 illustrates the result of such kinetic analysis in Ar, Kr, and Xe matrixes.

The dominating photodissociation products of HCOF at 193 and 248 nm are the CO/HF species in all matrixes. In argon matrix the growth of the CO/HF species follows first-order kinetics, and shows nearly perfect correlation with the decay of the precursor (Figure 8). In krypton and xenon matrixes, however, also the CO/HF species were bleached at both wavelengths. By assuming first-order kinetics with two steps, i.e.

$$A_1 \xrightarrow{k_1} A_2 \xrightarrow{k_2} \text{products} \tag{6}$$

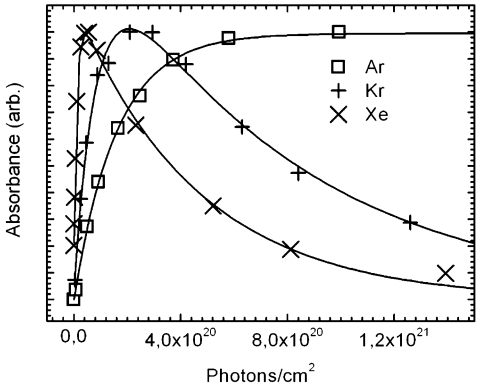

Figure 8. Evolution of the integrated absorbance of the HF/CO species upon photolysis at 248 nm. The argon matrix data is fitted to simple first-order kinetics, whereas for krypton and xenon a two-step mechanism of eq 7 is used. All samples have an initial dilution ratio of 1/2000.

the data can be fitted to a formula

$$A_2 = A_2^{(0)} e^{-k_2 n} + \frac{k_1 A_1^{(0)}}{k_2 - k_1} (e^{-k_1 n} - e^{-k_2 n}) \qquad (7)$$

where A_2 is the integrated absorbance of the CO/HF species, $A_2^{(0)}$ and $A_1^{(0)}$ represent the initial integrated absorbances of the CO/HF species and HCOF, respectively. k_1 and k_2 are cross sections for decay of HCOF and CO/HF species, respectively. The cross sections obtained by fitting the data to the first-order kinetics are collected in Table 2 and the corresponding fits are shown in Figure 8. It should be noted, that 248 nm photolysis was carried out in Kr matrix with several laser pulse energies and no indication of two photon nature of photodissociation of HCOF or CO/HF species was observed.

Computational Results

The computed properties of CO, HF, CO−HF, and OC−HF are collected in Table 3. The CO−HF and OC−HF complexes possess linear structures. The bond distances, harmonic frequencies, and vertical excitation energies of CO and HF molecules were obtained at the CCSD and B3LYP levels with satisfactory accuracy. The CIS calculations typically underestimate bond distances and overestimate harmonic frequencies of diatomic molecules.[37] In the CO/HF complexes the CO and HF bond distances are typically shifted less than 0.01 Å. The vertical excitation energies of the CO/HF complexes are very close to values of the CO molecule, and the nature of the excitation is almost purely CO excitation. The harmonic frequencies of CO/HF complexes are also shifted from the values of CO and HF molecules.

Discussion

The photodissociation efficiency of HCOF at 248 nm depends strongly on the matrix host. As seen in Table 2, dissociation in xenon matrix is characterized by a significantly larger cross-section than in argon or in krypton matrixes, where the cross sections are, within experimental uncertainty, of the same order of magnitude. This observation is in accordance with our previous results for formaldehyde in rare gas matrixes.[3] To clarify this phenomenon we next discuss the results of the photodissociation of HCOF in solid rare gas matrixes.

UV excitation within the first excited singlet state of HCOF is followed by different decay mechanisms. Intersystem crossing to the first triplet state leads to both C−F and C−H bond cleavage from which the latter has larger rate coefficient.[11] The dissociation energy via channel 2 is estimated to be 418 kJ/mol (4.3 eV/molecule), which provides excess energy of 0.7 and 2.1 eV to be partitioned among the fragments upon photoexcitation at 248 and 193 nm, respectively.[8−10] As discussed in ref 11, the C−F bond cleavage can also occur on the excited singlet surface at excitation wavelength shorter than 233 nm.

In argon matrix, the primary photodissociation products at 248 and 193 nm are the thermally unstable CO/HF species and only minor amount of stable CO−HF and OC−HF complexes is formed. In the gas phase, channel 2 on the T_1 surface and channel 3 on the S_1 surface dominate and it is estimated that ∼49% and ∼40−46% of the total excess energy involved in dissociation via channels 2 and 3, respectively, is released as translational energy. As a light particle, hydrogen atom adopts nearly all of this energy. In a solid matrix the separation of the photodissocation products is hindered by cage effect,[40] and the kinetic energy of ∼1 eV of the hot hydrogen atom is well below the threshold ∼1.7 eV needed for successful cage exit in argon matrix.[41] On the basis of these arguments, the absence of the FCO radical in our Ar matrix spectra is not surprising. Similarly, the cage effect prevents the F atom cage exit[42] in channel 3 on S_1 and T_1 surfaces in argon matrix. The even smaller excess energy provided by 248 nm excitation would not support cage exit of atomic fragments in the photolysis. The mechanism responsible for formation of matrix isolated CO in the photo-

TABLE 2: Photodissociation Cross Sections (in cm²)

	248 nm			193 nm		
	$k/10^{-21}$	$k_1/10^{-21}$	$k_2/10^{-21}$	$k/10^{-21}$	$k_1/10^{-21}$	$k_2/10^{-21}$
Ar[a]	5.4	6.4		300	340	
Ar[b]	12	12				
Ar[c]	8.7	9.9				
Kr[a]	13	12	1.3	240	210	3.5
Xe[a]	67	85	2.2	360[d]	110	15

[a] Dilution ratio 1/2000. [b] Dilution ratio 1/5000. [c] Dilution ratio 1/500. [d] Non-first-order-kinetics. The data points were fitted by assuming first-order kinetics at an early stage of the photolysis.

TABLE 3: Computed Ground State Bond Distances (in Å), Harmonic Frequencies (in cm⁻¹), and Vertical Excitation Energies (in eV)

	CIS	EOM-CCSD	TD-B3LYP	expt[38]
		CO		
r_{CO}	1.1053	1.1301	1.1277	1.1281
ν_{CO}	2432	2226	2212	2143
ΔE_v	9.450	8.801	8.415	8.52
		HF		
r_{HF}	0.8975	0.9139	0.9222	0.9170
ν_{HF}	4492	4227	4096	3858.56
ΔE_v	11.915	10.246	9.668	10.06[a]
		CO−HF		
r_{CO}	1.1076	1.1320	1.1298	
r_{HF}	0.8988	0.9148	0.9243	
r_{OH}	2.1763	2.1499	2.0736	
ν_{CO}	2411	2212	2195	2129.31[b]
ν_{HF}	4465	4218	4054	3908.44[b]
ΔE_v	9.294	8.825	8.418	
		OC−HF		
r_{CO}	1.1025	1.1271	1.1241	
r_{HF}	0.9002	0.9178	0.9302	
r_{CH}	2.3230	2.1836	2.0587	
ν_{CO}	2460	2253	2246	2162.31[b]
ν_{HF}	4423	4142	3907	3789.39[b]
ΔE_v	9.578	9.048	8.061	

[a] Full CI estimate from ref 39. [b] Our experiments in argon matrix.

dissociation of HCOF in argon matrix is not clear, however, at least two processes should be considered. First, the gas phase study of ref 12 indicates that channel 1, producing HF + CO, has a very small branching ratio of ~0.06 at 193 nm, and only ~1 eV of the excess energy is released as translational energy. Although the cage exit thresholds for CO or HF have not been quantified, it seems evident that channel 1 cannot provide cage exit of the molecular fragment. Second, dissociation of HCOF dimers and higher aggregates present in the samples may provide dissociation channels favoring formation of carbon monoxide. Although the source for carbon monoxide is unknown, it is formed via a channel with minor importance. The kinetic analysis shows that the decay of HCOF and the formation of CO/HF species have equal cross sections in argon matrix, which supports the fact that cage exit of atoms produced via channels 2 and 3 does not take place in argon matrix upon photodissociation at 248 and 193 nm. Thus, formation of CO/HF species is ascribed to in-cage reaction of the fragments, i.e., H + FCO, F + HCO and HF + CO.

Photodissociation of HCOF at 248 and 193 nm in krypton matrix yielded a variety of photoproducts. Comparison of the photodissociation efficiencies shows that the decay of HCOF has slightly larger cross-section than the growth of CO/HF species. This observation can be regarded as an evidence of atomic cage exit upon photoexcitation at these wavelengths. The cross-section for formation of the FCO radical is estimated to be 4.6×10^{-21} cm^2, which is larger than the decay cross section of CO/HF species (1.3×10^{-21} cm^2), and it is too large to fulfill the relation $k_{HCOF} = k_{HF/CO} + k_{FCO}$, where k_{HCOF} is the cross section of decay of HCOF and $k_{HF/CO}$, and k_{FCO} are growth cross sections of CO/HF species and FCO, respectively. However, the CO/HF species cross-section is most probably overestimated by some extent, because the HCOF dimers and higher aggregates might also produce CO/HF species, which is demonstrated in argon matrix. Of course, the FCO cross-section may be overestimated by the same reason. The cross sections of the growth of HF, CO, and Kr_2H^+ are all estimated to be 10^{-21} cm^2, which correlates rather closely with disappearance of the CO/HF species. On the other hand, the cross-section for formation of F_2CO is 3 orders of magnitude smaller, and its formation may probably be related to reaction between FCO and photomobile fluorine atom.[43] This is still somewhat unclear, because we have not observed disappearance of FCO upon photolysis at 248 nm. More clear evidence of atomic cage exit is provided by the UV absorption of F atoms in a krypton matrix and by the IR observation of HKrF and HCO upon annealing of extensively photolyzed samples. A rough quantitative estimate for the H atom cage exit probability can be provided by assuming a cross-section $k_{HCOF} - k_{CO/HF} = 1 \times 10^{-21}$ cm^2. This would imply a quantum yield less than 0.01 for the H atom cage exit via channel H + FCO in krypton matrix. Obviously, the photochemistry of CO/HF species has to be studied more carefully in order to provide more precise picture of photodissociation of HCOF in krypton matrix. It should be noted, that the excess energies needed for H and F atom cage exit are comparable in krypton and argon matrixes.[41,44]

The nonfirst-order kinetics of HCOF decay in a xenon matrix indicates that secondary photoinduced effects may take place upon photolysis at 193 nm. The appearance of FCO and some evidence of the HCO radical indicate formation of H and F atoms upon photolysis. In a xenon matrix the photoinduced mobility of atoms may cause reactions when those come across molecular species. However, primary photodissociation of HCOF in xenon may not lead to permanent separation of dissociated species in important quantity. This is supported by comparison of cross sections, which indicates negligible probability for atomic cage exit at 248 nm.

The efficient formation of CO/HF species in argon, krypton, and xenon matrixes clearly indicates a small cage exit probability of the photolysis products. In the gas phase, channel 1 has quantum yield of ~0.06 and <0.20 at 193 and 250 nm, respectively.[12,10] This leads to conclusion that other dissociation channels than channel 1 contribute in production of CO/HF species, which then thermally relax into well-defined CO−HF and OC−HF configurations. One possible scheme for CO/HF species formation at 193 nm photolysis can be introduced as a stepwise process:

$$\mathrm{HCOF} \xrightarrow{h\nu} \mathrm{HCOF}^* \xrightarrow{\phi_1} \mathrm{HF} + \mathrm{CO} \xrightarrow{\phi_1} \mathrm{CO/HF} \quad (8)$$

$$\xrightarrow{\phi_2} \mathrm{H} + \mathrm{FCO} \xrightarrow{\phi_2'} \mathrm{H} + \mathrm{FCO} \quad (9)$$

$$\xrightarrow{\phi_2''} \mathrm{HCOF} \quad (10)$$

$$\xrightarrow{\phi_2'''} \mathrm{CO/HF} \quad (11)$$

$$\xrightarrow{\phi_3} \mathrm{F} + \mathrm{HCO} \xrightarrow{\phi_3'} \mathrm{F} + \mathrm{HCO} \quad (12)$$

$$\xrightarrow{\phi_3''} \mathrm{HCOF} \quad (13)$$

$$\xrightarrow{\phi_3'''} \mathrm{CO/HF} \quad (14)$$

where ϕ_i represents quantum yield of the corresponding step. Step 8 describes the direct molecular dissociation channel 1, in which permanent separation of molecules is prevented by matrix cage effect (see above discussion). Steps 12 and 13 represent dissociation channel 3, which could lead to F atom permanent cage exit (step 12) and/or in-cage reaction between H and HCO, and formation of vibrationally excited HCOF molecule as a reaction intermediate.[45] Subsequently, vibrationally excited intermediate HCOF molecule can dissociate and produce vibrationally excited HF and CO molecules[6,45] (step 14), or they might undergo cooling by vibrational relaxation in the matrix cage (step 13). Although, detailed reaction mechanism of the H + FCO → HF + CO reaction[46] and the possible reaction intermediate are, according to our knowledge, not reported in the literature, we tentatively assume that the H + FCO reaction proceeds via mechanism similar to the F + HCO case. This clearly leads to complex dissociation kinetics, which cannot be solved with parameters extracted from the present experiments. To make a rough estimate of how much ϕ_2'' would affect the total photodissociation cross-section, k (see eq 5 and Table 2), of HCOF at 248 nm, we adopted quantum yields ϕ_1 and ϕ_2 from gas-phase results[10] and set $\phi_3 = 0$. Then we varied ϕ_2'' between $0 \le \phi_2'' \le \phi_2$ and recorded variation of the cross-section, which was orders of magnitude too small to explain the observed variation of the photodissociation cross-section in different rare gas matrixes.

The more efficient photodissociation of HCOF at 193 nm can be explained by comparing the gas-phase absorption cross sections of $\tilde{A}(^1A'') \leftarrow \tilde{X}(^1A')$ transition of HCOF[35] at ~193 nm and at ~248 nm. Although the ratio of the cross sections $\sigma_{\sim 193nm}/\sigma_{\sim 248nm} = 9 \times 10^{-19}/5 \times 10^{-21} = 180$ in the gas phase is relatively far from the ratio of photodissociation cross sections obtained in our experiments, $k^{Ar}_{193nm}/k^{Ar}_{248nm} = 56$ and $k^{Kr}_{193nm}/k^{Kr}_{248nm} = 19$, it should be noted that matrixes are always scattering, which would decrease the effective fluency in particular at short wavelengths, and thus lead to somewhat

smaller k_{193nm}/k_{248nm} ratio. This is clearly demonstrated in UV absorption spectrum of HCOF in argon matrix, where absorbance at 193 nm is orders of magnitude larger than at 248 nm. Moreover, the UV absorption spectra of polyatomic molecules embedded in solid matrixes are shifted from the gas phase by some extent. The absorption cross section of HCOF increases relatively steeply from 248 nm to shorter wavelengths, and at ~228 nm the cross-section is already order of magnitude larger. Consequently, a red shift of ca. 20 nm from argon to xenon matrix might be sufficient to explain the observed faster kinetics in xenon matrix. However, the UV absorption spectra of HCOF do not support this assumption.

An interesting observation in the course of this study was the photodissociation of CO/HF species in heavier rare gas matrixes. This is quite unexpected since the first excited singlet states of CO and HF molecules are not energetically accessible with 193 and 248 nm photons. It should be noted that according to our experiments, isolated HF does not dissociate in krypton matrix upon 193 nm photolysis. Nevertheless, the CO/HF species were effectively bleached at both wavelengths in krypton and xenon matrixes. In krypton matrix, experiments with different pulse energies at 248 nm clearly exclude the role of two photon absorption in the photochemistry of CO/HF species. On the other hand, quantum chemical calculations of vertical excitation energies of CO−HF and OC−HF complexes indicate that the first excited states of CO and HF are only slightly perturbed in these complexes. This supports the fact that solid environment promotes photodissociation of CO/HF in krypton and xenon matrices at these excitation energies. In rare gas matrices photon-induced dissociation can proceed via electronic excitation of rare gas host followed by exciton transport and subsequent localization at molecular impurity sites, which may then lead to dissociation of the molecular impurity.[40] In solid krypton, the excitonic bands are accessible via two-photon excitation at photon energies near 5 eV. Apart from excitonic processes, harpoon reactions in condensed phase provide a channel for impurity molecule dissociation. In harpoon reactions excitation onto guest−host potential might lead to photodissociation of the guest molecules. This is well characterized in a hydrogen halide doped xenon matrix.[47] However, both processes involve multiphoton excitation, which is not consistent with our observation that photodissociation of CO/HF in krypton is a single photon process. Of course, excitation within the intermolecular potential of geminate guests,[48] i.e., CO and HF, could in principle provide a channel for photodissociation. However, our ab initio calculations indicate that transition to the lowest excited state of CO/HF complex is energetically inaccessible to at 248 and 193 nm. It should be noted that the present calculations deal with the CO/HF pair only, and therefore, the effects of the solid environment are neglected. To shed more light into the mechanism responsible for dissociation, more rigorous theoretical treatment including condensed phase effects is clearly needed. An important input for such treatment is provided by the experimental observation that FCO is formed in the photolysis of CO/HF species indicating H atom cage exit and, thus, phodissociation of HF. It is noteworthy that the structure of thermally unstable CO/HF is not known and it is possible that it could be a metastable reaction intermediate such as an isomer of HCOF. However, photodissociation of the CO/HF complex as well as the thermally unstable CO/HF species was observed in krypton and in xenon matrixes.

Conclusions

In this study the UV photodissociation of HCOF was investigated in argon, krypton, and xenon matrixes at 193 and 248 nm. The main goal of the study was to extend our knowledge of the condensed phase effects on photodissociation of polyatomic molecules. In all matrixes, the photodissociation of HCOF lead to efficient formation of CO/HF species, which can be taken as an evidence of negligible atomic cage exit upon photodissociation. In argon matrix, the CO/HF species were annealed to stable CO−HF and OC−HF structures. In krypton and xenon matrixes, these two stable geometries were not as evident as in argon but some spectral assignment were given. Interestingly, the CO/HF species were further dissociated in krypton and xenon matrices, but not in argon. Photon energies at 248 and 193 nm are well below energies needed to photodissociation of CO and HF. Experiments showed that photodissociation of CO/HF species are single photon processes. Quantum chemical calculations of excitation energies of CO−HF and OC−HF complexes indicated that the first excited states of both molecules are only slightly perturbed in the CO/HF complex. These observations lead to conclusion that photodissociation of CO/HF complexes in rare gas matrixes is promoted by the solid environment. The photomobile atoms might also play some role in the observed photochemistry.

References and Notes

(1) Van Zee, R. D.; Foltz, M. F.; Moore, C. B. *J. Chem. Phys.* **1993**, *99*, 1664. Feller, D.; Dupuis, M.; Garrett, B. C. *J. Chem. Phys.* **2000**, *113*, 218. Yin, H.-M.; Nauta, K.; Kable, S. H. *J. Chem. Phys.* **2005**, *122*, 194312-1 and references therein.

(2) Thomas, S. G.; Guillory, W. A. *J. Phys. Chem.* **1973**, *77*, 2469.

(3) Vaskonen, K. J.; Kunttu, H. M. *J. Phys. Chem. A* **2003**, *107*, 5881 and references therein.

(4) Wallington, T. J.; Hurley, M. D.; Fracheboud, J. M.; Orlando, J. J.; Tyndall, G. S.; Sehested, J.; Møgelberg, T. E.; Nielsen, O. J. *J. Phys. Chem.* **1996**, *100*, 18116 and references therein.

(5) Klimek, D. E.; Berry, M. J.*Chem. Phys. Lett.* **1973**, *20*, 141.

(6) Choi, Y. S.; Moore, C. B. *J. Chem. Phys.* **1992**, *97*, 1010.

(7) Weiner, B. R.; Rosenfeld, R. N. *J. Phys. Chem.* **1988**, *92*, 4640.

(8) Maul, C.; Dietrich, C.; Haas, T.; Gericke, K.-H.; Tachikawa, H.; Langford, S. R.; Kono, M.; Reed, C. L.; Dixon, R. N.; Ashfold, M. N. R. *Phys. Chem. Chem. Phys.* **1999**, *1*, 767.

(9) Reed, C. L.; Kono, M.; Langford, S. R.; Hancock, W. R.; Dixon, R. N.; Ashfold, M. N. R. *J. Chem. Soc., Faraday Trans.* **1997**, *93*, 2721. Reed, C. L.; Kono, M.; Langford, S. R.; Hancock, W. R.; Dixon, R. N.; Ashfold, M. N. R. *J. Chem. Phys.* **1997**, *106*, 6198.

(10) Hancock, T. W. R.; Dixon, R. N. *J. Chem. Soc., Faraday Trans.* **1997**, *93*, 2707.

(11) Fang, W.-H.; Liu, R.-Z. *J. Chem. Phys.* **2001**, *115*, 5411.

(12) Lee, S.-H.; Wu, C.-Y.; Yang, S.-K.; Lee, Y.-P. *J. Chem. Phys.* **2005**, *123*, 074326.

(13) Shatte, G.; Willner, H.; Hoge, D.; Knözinger, E.; Schrems, O. *J. Phys. Chem.* **1989**, *93*, 6025.

(14) Olah, G. A.; Kuhn, S. J. *J. Am. Chem. Soc.* **1960**, *82*, 2380.

(15) Gaussian 03, Revision C.02, Frisch, M. J.; Trucks, G. W.; Schlegel, H. B.; Scuseria, G. E.; Robb, M. A.; Cheeseman, J. R.; Montgomery, J. A., Jr.; Vreven, T.; Kudin, K. N.; Burant, J. C.; Millam, J. M.; Iyengar, S. S.; Tomasi, J.; Barone, V.; Mennucci, B.; Cossi, M.; Scalmani, G.; Rega, N.; Petersson, G. A.; Nakatsuji, H.; Hada, M.; Ehara, M.; Toyota, K.; Fukuda, R.; Hasegawa, J.; Ishida, M.; Nakajima, T.; Honda, Y.; Kitao, O.; Nakai, H.; Klene, M.; Li, X.; Knox, J. E.; Hratchian, H. P.; Cross, J. B.; Bakken, V.; Adamo, C.; Jaramillo, J.; Gomperts, R.; Stratmann, R. E.; Yazyev, O.; Austin, A. J.; Cammi, R.; Pomelli, C.; Ochterski, J. W.; Ayala, P. Y.; Morokuma, K.; Voth, G. A.; Salvador, P.; Dannenberg, J. J.; Zakrzewski, V. G.; Dapprich, S.; Daniels, A. D.; Strain, M. C.; Farkas, O.; Malick, D. K.; Rabuck, A. D.; Raghavachari, K.; Foresman, J. B.; Ortiz, J. V.; Cui, Q.; Baboul, A. G.; Clifford, S.; Cioslowski, J.; Stefanov, B. B.; Liu, G.; Liashenko, A.; Piskorz, P.; Komaromi, I.; Martin, R. L.; Fox, D. J.; Keith, T.; Al-Laham, M. A.; Peng, C. Y.; Nanayakkara, A.; Challacombe, M.; Gill, P. M. W.; Johnson, B.; Chen, W.; Wong, M. W.; Gonzalez, C.; and Pople, J. A. Gaussian, Inc.: Wallingford CT, 2004.

(16) Schmidt, M. W.; Baldridge, K. K.; Boatz, J. A.; Elbert, S. T.; Gordon, M. S.; Jensen, J.; Koseki, S.; Matsunaga, N.; Nguyen, K. A.; Su, S.; Windus, T. L.; Dupuis, M.; Montgomery, J. A. *J. Comput. Chem.* **1993**, *14*, 1347.

(17) Becke, A. D. *J. Chem. Phys.* **1993**, *98*, 5648.

(18) Purvis, G. D., III; Bartlett, R. J. *J. Chem. Phys.* **1982**, *76*, 1910.

(19) Foresman, J. B.; Head-Gordon, M.; Pople, J. A.; Frisch, M. J. *J. Phys. Chem.* **1992**, *96*, 135.

(20) Casida, M. E.; Jamorski, C.; Casida, K. C.; Salahub, D. R. *J. Chem. Phys.* **1998**, *108*, 4439.
(21) Stanton, J. F. *J. Chem. Phys.* **1993**, *99*, 8840.
(22) Krishnan, R.; Binkley, J. S.; Seeger, R.; Pople, J. A. *J. Chem. Phys.* **1980**, *72*, 650.
(23) Ahokas, J.; Vaskonen, K.; Kunttu, M. To be published.
(24) Dubost, H. *Chem. Phys.* **1976**, *12*, 139.
(25) Mason, M. G.; Von Holle, W. G.; Robinson, D. W. *J. Chem. Phys.* **1971**, *54*, 3491.
(26) Andrews, L.; Johnson, G. L. *J. Phys. Chem.* **1984**, *88*, 425.
(27) Jacox, M. E. *J. Mol. Spectrosc.* **1980**, *80*, 257.
(28) Bouteiller, Y.; Abdelaoui, O.; Schriver, A.; Schriver-Mazzuoli, L. *J. Chem. Phys.* **1995**, *102*, 1731.
(29) Kunttu, H. M.; Seetula, J. A. *Chem. Phys.* **1994**, *189*, 273.
(30) Irvine, M. J.; Mathieson, J. G.; Pullin, A. D. E. *Aust. J. Chem.* **1982**, *35*, 1971.
(31) Pettersson, M.; Khriachtchev, L.; Lignell, A.; Räsänen, M.; Bihary, Z.; Gerber, R. B. *J. Chem. Phys.* **2002**, *116*, 2508.
(32) Milligan, D. E.; Jacox, M. E. *J. Chem. Phys.* **1969**, *51*, 277.
(33) Pettersson, M.; Khriachtchev, L.; Jolkkonen, S.; Räsänen, M. *J. Phys. Chem. A* **1999**, *103*, 9154.
(34) Kunttu, H.; Seetula, J.; Räsänen, M.; Apkarian, V. A. *J. Chem. Phys.* **1992**, *96*, 5630.
(35) Giddings, L. E., Jr.; Innes, K. K. *J. Mol. Spectrosc.* **1961**, *6*, 528.
(36) Kunttu, H.; Feld, J.; Alimi, R.; Becker, A.; Apkarian, V. A. *J. Chem. Phys.* **1990**, *92*, 4856.
(37) Stanton, J. F.; Gauss, J.; Ishikawa, N.; Head-Gordon, M. *J. Chem. Phys.* **1995**, *103*, 4160.
(38) Hertzberg, G. *Spectra of Diatomic Molecules*; Van Nostrand: New York, 1950.
(39) Bettendorff, M.; Buenker, R. J.; Peyerimhoff, S. D.; Römelt, J. *Z Phys. A* **1982**, *304*, 125.
(40) Apkarian, V. A.; Schwentner, N. *Chem. Rev.* **1999**, *99*, 1481.
(41) Schriever, R.; Chergui, M.; Ünal, Ö.; Schwentner, N.; Stepanenko, V. *J. Chem. Phys.* **1990**, *93*, 245.
(42) Feld, J.; Kunttu, H.; Apkarian, V. A. *J. Chem. Phys.* **1990**, *93*, 1009.
(43) Kunttu, H.; Sekreta, E.; Apkarian, V. A. *J. Chem. Phys.* **1991**, *94*, 7819.
(44) Kunttu, H, Apkarian, V. A. *Chem. Phys. Lett.* **1990**, *171*, 423.
(45) Donaldson, D. J.; Sloan, J. J. *J. Chem. Phys.* **1985**, *82*, 1873.
(46) Gangloff, H. J.; Milks, D.; Maloney, K. L.; Adams, T. N.; Matula, R. A. *J. Chem. Phys.* **1975**, *64*, 4915.
(47) Fajardo, M. E.; Apkarian, V. A. *J. Chem. Phys.* **1988**, *89*, 4102.
(48) Gudipati, M. S. *J. Phys. Chem. A* **1997**, *101*, 2003.